An Alternative Efficient Redox Couple for the Dye-Sensitized Solar Cell System

Hervé Nusbaumer,* Shaik M. Zakeeruddin, Jacques-E. Moser, and Michael Grätzel[a]

Abstract: A series of new cobalt complexes $[Co(LLL)_2X_2]$ were synthesized and evaluated as redox mediators for dye-sensitized nanocrystalline TiO_2 solar cells. The structure of the ligand and the nature of the counterions were found to influence the photovoltaic performance. The one-electron-transfer redox mediator $[Co(dbbip)_2](ClO_4)_2$ (dbbip = 2,6-bis(1′-butylbenzimidazol-2′-yl)pyridine) performed best among the compounds investigated. Photovoltaic cells incorporating this redox mediator yielded incident photon-to-current conversion efficiencies (IPCE) of up to 80%. The overall yield of light-to-electric power conversion reached 8% under simulated AM1.5 sunlight at 100 W m^{-2} intensity and more than 4% at 1000 W m^{-2}. Photoelectrodes coated with a 2 μm thick nanoporous layer and a 4 μm thick light-scattering layer, sensitized with a hydrophobic ruthenium dye, gave the best results.

Keywords: cobalt · redox chemistry · sensitizers · solar cells · tridentate ligands

Introduction

Nanocrystalline dye-sensitized solar cells (DSSC) are attracting great interest because of their high efficiency and potential applications as cost-effective alternatives to present day $p-n$ junction photovoltaic devices. In the conventional systems the semiconductor takes on the tasks of light absorption and charge-carrier transport, whereas these two functions are separated in DSSCs. A sensitizer anchored to the surface of a TiO_2 semiconductor absorbs the light, and charge separation occurs at the interface by photo-induced electron injection from the dye into the conduction band of TiO_2. Carriers are transported in the conduction band of the semiconductor to the charge collector. The use of ruthenium complexes as sensitizers having a broad absorption band in conjunction with oxide films of nanocrystalline morphology permits a large fraction of sunlight to be harvested. After charge injection, the original state of the sensitizer is subsequently restored by electron donation from an electrolyte-containing redox system such as the triiodide/iodide couple. After donating an electron to the sensitizer the iodide ion is regenerated in turn by reduction of a triiodide ion at the counterelectrode, the circuit being completed by diffusion of the iodide ion back to the dye-sensitized photoanode (Figure 1).

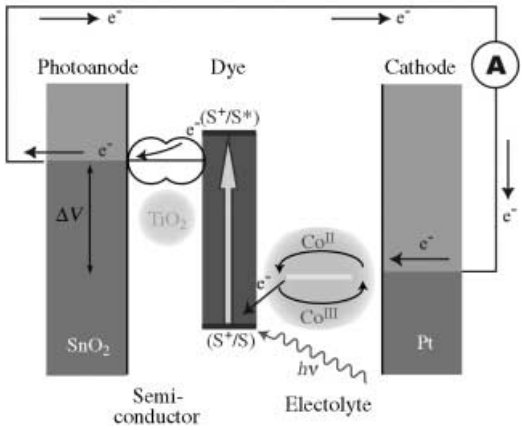

Figure 1. Schematic of operation of the dye-sensitized electrochemical photovoltaic cell. The photoanode receives electrons from the photo-excited dye, which is thereby oxidized and in turn oxidizes the mediator dissolved in the electrolyte. The mediator is regenerated by reduction at the cathode by the electrons circulated through the external circuit.

A major research effort is under way to understand the parameters that control cell performance to improve the conversion efficiency and stability of DSSCs. Special attention has focused on development of sensitizers to harvest a larger region of the solar spectrum.[1–9] Efforts were made to develop highly porous nanostructured films consisting of an oxide semiconductor with a wide band gap.[10–14] Attempts are also in progress to optimize the redox electrolyte,[15–23] electron transport in the TiO_2 film,[24–26] and dye stability.[27–29] Triiodide/iodide is the common choice of redox couple for obtaining high efficiencies in liquid electrolytes.[30, 31] Despite

[a] H. Nusbaumer, Dr. S. M. Zakeeruddin, PD Dr. J.-E. Moser, Prof. Dr. M. Grätzel
Laboratory for Photonics and Interfaces
Institute of Molecular and Biological Chemistry
Swiss Federal Institute of Technology, 1015 Lausanne (Switzerland)
Fax: (+41)21-693-4111
E-mail: herve.nusbaumer@epfl.ch

  DOI: 10.1002/chem.200204577

its good performance, the triiodide/iodide couple has its own disadvantages: the triiodide ion absorbs a significant part of the visible light when employed in high concentrations, its low redox potential limits the open-circuit voltage available, and its aggressiveness towards silver prevents the use of this metal as current collector in large cells.

Here we continue our earlier work[21] introducing cobalt complexes instead of triiodide/iodide as redox mediators in dye-sensitized solar cells. After screening a series of candidates, $[Co(dbbip)_2](ClO_4)_2$ was identified as the most promising and became the focus of further investigations. This complex was characterized and used for detailed photovoltaic studies. These include changes in dye design, the structure of the TiO_2 film, the nature of the counterelectrode, the concentration of the redox mediator in the reduced and oxidized states, and the influence of additives. While preparing this manuscript an article appeared on cobalt complexes of commercially available ligands.[32] These cobalt redox couples are not as efficient as the complexes presented here, mainly due to their low redox potentials.

Results and Discussion

Screening of redox couples: The cobalt complexes listed in the Experimental Section were screened to identify the most promising candidates for use as redox mediators in DSSC. Data on the photovoltaic performance, such as the incident photon-to-current conversion efficiencies (IPCE) at 540 nm and efficiencies obtained with these redox electrolytes, is compiled in Table 1, together with their measured redox potentials. The complexes $[Co(dbbip)_2](ClO_4)_2$ and $[Co(dmbip)_2](ClO_4)_2$ showed the best performance.

Table 1. Photovoltaic data for from various cobalt complexes for an illumination of 100 W m^{-2}.

Redox mediator	V_{OC} [mV]	J_{SC} [μA cm^{-2}]	J_{SC}[a] [mA cm^{-2}]	FF	Efficiency [%]	IPCE[b] [%]	$E_{1/2}$ [V]
$[Co(terpy)_2](ClO_4)_2$	470	130	1.4	0.70	0.5	11	0.25
$[Co(bipy)_3](ClO_4)_2$	510	280	3.1	0.73	1.1	18	0.30
$[Co(phen)_3](OTf)_2$	600	250	3.0	0.75	1.2	16	0.36
$[Co(dbbip)_2](ClO_4)_2$	660	800	6.5	0.76	4.2	38	0.39
$[Co(dmbip)_2](ClO_4)_2$	650	520	4.2	0.76	2.7	25	0.44
$[Co(dmbip)_2](DDS)_2$	650	200	2.4	0.73	1.0	11	0.45
$[Co(dmbip)_2](PF_6)_2$	640	350	3.8	0.75	1.8	17	0.45

[a] At 1000 W m^{-2}. [b] IPCE at 540 nm.

Since the conduction band edge of the photoanode (dye-coated TiO_2 film) is independent of the redox couple, and the Fermi level of the counterelectrode is close to the redox potential, a considerable increase in the open-circuit voltage V_{OC} could be achieved by using a couple of higher redox potential than that of I_3^-/I^-. Nevertheless, there should be adequate potential difference between the dye and the redox couple to provide a driving force for Co^{II} to regenerate the oxidized state of the dye. The influence of the potential of the redox mediator on the V_{OC} of the CSSC can be clearly seen in Table 1. Increasing the redox-couple potential $E_{1/2}$ by 0.2 V, from $[Co(terpy)_2](ClO_4)_2$ to $[Co(dmbip)_2](ClO_4)_2$, results in an increase in V_{OC} of 0.18 V, as expected. Surprisingly Sapp et al.[32] did not observe any correlation between V_{OC} and $E_{1/2}$ for the series of cobalt complexes they investigated.

We also compared the influence of ClO_4^-, OTf^-, PF_6^-, and DDS^- counterions on the photovoltaic performance of $[Co(dmbip)_2]^{2+}$. No difference was found in the redox potentials of $[Co(dmbip)_2]^{2+}$ complexes when the counterion was varied. Interestingly, although significant differences were found for IPCE and the short-circuit current J_{SC}, hardly any differences in V_{OC} were noted (Table 1). The variation in J_{SC} may be due to the association of the anion with the electroactive cobalt complex, which affects the rate of electron transfer from the latter to the oxidized dye.

The incident light power, or irradiance, on the DSSC surface is expressed in watts per square meter; 1000 W m^{-2} is equivalent to the full power of the sun (100% sun) for an air-mass number of 1.5 (AM1.5). The photovoltaic efficiency of a DSSC with the complex $[Co(dbbip)_2](ClO_4)_2$ at 100 W m^{-2} (10% sun) was superior to those of all other redox mediators. Hence, $[Co(dbbip)_2](ClO_4)_2$ was used for further investigations. In the photovoltaic measurements, linearity between illumination intensity and photocurrent was not attained due to mass-transfer limitations of the photocurrent, which is limited by Co^{III} diffusion to the counterelectrode at higher light intensity. The small superlinearity sometimes observed between the photocurrent densities at 100 W m^{-2} and 1000 W m^{-2}, whereby J_{SC} at 100% sun (1000 W m^{-2}) is slightly higher than ten times J_{SC} at 10% sun, is due to approximate values at lower irradiance intensities, which are extrapolated to take into account the filters that are used in the experimental setup to decrease the incident light power.

Characterization of $[Co(dbbip)_2](ClO_4)_2$: $[Co(dbbip)_2](ClO_4)_2$ was characterized by ^1H and ^{13}C NMR spectroscopy, UV/Vis spectrophotometry, elemental analysis, and electrochemical methods. Elemental analysis (%) calculated for $C_{54}H_{58}N_{10}CoCl_2O_8$ (1104.97): C 58.70, H 5.29, N 12.68; found: C 58.64, H 5.26, N 12.59. The ^1H NMR spectra of $[Co(dbbip)_2](ClO_4)_2$ in CD_3CN showed broad peaks due to the paramagnetic nature of Co^{2+}, whereas the oxidized complex shows two sets of sharp peaks corresponding to the aliphatic and aromatic protons of the dbbip ligand: aliphatic part: $\delta =$ 4.86 (t, 8H), 1.83 (m, 8H), 1.11 (m, 8H), 0.69 (t, 12H); aromatic part: $\delta = 9.46$ (t, 2H), 9.16 (d, 4H), 7.64 (d, 4H), 7.43(t, 4H), 7.28 (t, 4H), 5.77 (d, 4H). In the ^{13}C NMR spectrum 14 signals were found at $\delta = 151.6$, 149.1, 148.1, 136.9, 136.8, 128.5, 128.2, 127.9, 114.3, 114.2, 46.9, 31.9, 19.7, and 13.1 ppm.

In the crystal structure of $[Co(dbbip)_2](ClO_4)_2$, the unit cell contains two symmetry-independent $[Co(dbbip)_2]^{n+}$ cations (Figure 2),[33] which have different conformations due to disorder in the *n*-butyl chains. The geometry of the $[Co(dbbip)_2]^{n+}$ ion can be described by a distorted octahedral environment of six nitrogen atoms. The bond lengths and bond angles were averaged within the idealized D_2 symmetry. The crystal consists of layers of $[Co(dbbip)_2]^{n+}$ ions packed parallel to the *ab* plane with ClO_4^- ions between the layers. The closest Co···Co distance between neighboring cations in

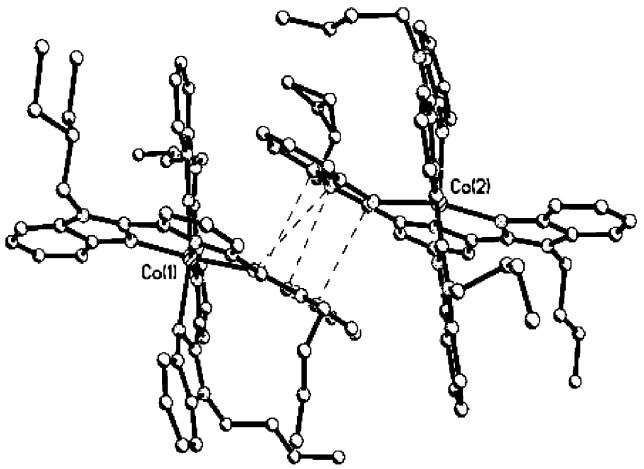

Figure 2. A quasicentrosymmetric pair of crystallographically independent $[Co^{II}(dbbip)_2]^{2+}$ ions.

a layer is 8.42 Å. It is noteworthy that *n*-butyl chains of the $[Co(dbbip)_2]^{n+}$ moieties point towards the neighboring cationic layer.

One of the conditions for the electrolyte to be suitable for use in DSSC is that the light absorption of the oxidized and reduced forms in the visible region should be as low as possible, especially for illumination from the counterelectrode side. Only then can most of the visible light reach the photoelectrode. The dye has an absorption maximum in the visible region at about 530 nm in acetonitrile; hence, the extinction coefficient of the electrolytic solution should be a minimum around that wavelength. $[Co^{II}(dbbip)_2]^{2+}$ was characterized by NMR spectroscopy and UV/Vis spectrometry, and after complete oxidation to Co^{III}, $[Co^{III}(dbbip)_2]^{3+}$ was characterized by NMR spectroscopy and spectrophotometry. The UV/Vis spectra shown in Figure 3 indicate that the

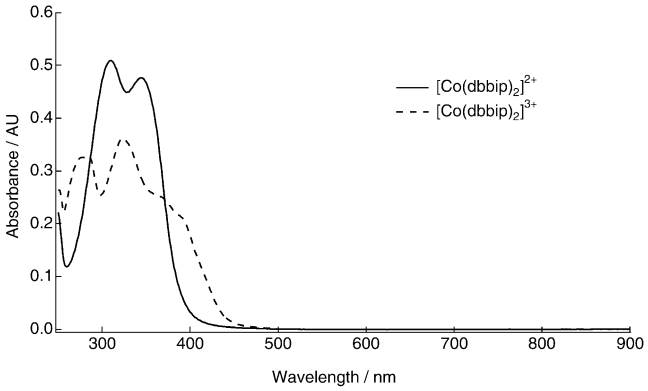

Figure 3. UV/Vis spectra of $[Co^{II}(dbbip)_2]^{2+}$ and $[Co^{III}(dbbip)_2]^{3+}$ in acetonitrile (10^{-4} M).

complex has absorption maxima in the UV region in both oxidation states: λ_{max} (ε) = 310 (52000), 345 nm (50000) for $[Co^{II}(dbbip)_2]^{2+}$, and λ_{max} (ε) = 276 (44000), 323 nm (45000) for $[Co^{III}(dbbip)_2]^{3+}$. In the visible region, only the absorption tails remain, with $\varepsilon_{480}(Co^{II}) = 1.3 \times 10^2\,mol^{-1}\,dm^3\,cm^{-1}$ and $\varepsilon_{480}(Co^{III}) = 2.6 \times 10^2\,mol^{-1}\,dm^3\,cm^{-1}$. This weak absorption in the visible region allows the use of highly concentrated electrolytic solutions in counterelectrode-illuminated solar cells without significantly attenuating the visible light to be harvested by the sensitizer. Stationary amperometry was used to determine the standard redox potentials of the cobalt couples listed in Table 1 and the diffusion coefficient of $[Co(dbbip)_2](ClO_4)_2$, which was found to be $7.72 \times 10^{-6}\,cm^2\,s^{-1}$ in acetonitrile at 20 °C.

Electrolyte solutions were monitored with ^1H and ^{13}C NMR spectroscopy to reveal any chemical changes in the cobalt complex occurring as a consequence of adding such a strongly oxidizing agent as $NOBF_4$, used to convert Co^{II} to Co^{III}. Addition of $NOBF_4$ in stoichiometric amounts leads to total transformation of Co^{II} into Co^{III}. An excess of oxidizing agent attacked the dbbip ligand and caused degradation of the complex. As discussed below, a low Co^{III} concentration is required for high efficiency. As only about 10% of the complex was oxidized, no degradation problem was observed when using $NOBF_4$ as oxidizing agent.

Influence of the sensitizer: Solar cells based on electrolytes containing $[Co(dbbip)_2](ClO_4)_2$ and $[Co(dmbip)_2](ClO_4)_2$ redox systems were investigated with sensitizers *cis*-$[Ru^{II}$-(4,4′-dicarboxylate-*H*-2,2′-bipyridine)$_2$(NCS)$_2$](TBA)$_2$ (**1**), *cis*-$[Ru^{II}$(2,2′-bipyridine-4,4′-dicarboxylic acid)(4-methyl-4′-hexadecyl-2,2′-bipyridine)](NCS)$_2$ (**2**), and *cis*-$[Ru^{II}$(2,2′-bipyridine-4,4′-dicarboxylic acid)(4,4′-dinonyl-2,2′-bipyridine)]-(NCS)$_2$ (**3**). Adsorption of **1** onto the TiO_2 surface imparts a negative ξ potential to the nanocrystals.[34] By contrast, the heteroleptic complexes **2** and **3** carry two negative charges less than **1**, and this decreases the coulombic attraction between the adsorbed sensitizer and the positively charged cobalt complexes. This explains the pronounced differences in the photovoltaic behavior of these ruthenium dyes.

Preliminary screening of these three dyes with the cobalt redox electrolyte $[Co(dbbip)_2](ClO_4)_2$ showed that **1** gives inferior injection efficiencies and short-circuit photocurrent J_{SC} compared to **2** and **3**. The J_{SC} at full sun of **1** was about half of those of the the heteroleptic dyes. The superior performance of the heteroleptic dyes also manifests itself in the overall solar AM1.5 light-to-electric power conversion efficiencies. For **1**, **2**, and **3** the current–voltage ($I-V$) curves are compared in Figure 4. The power outputs of dyes **2** and **3** at the optimal power point exceed that of **1** by a factor of 2.

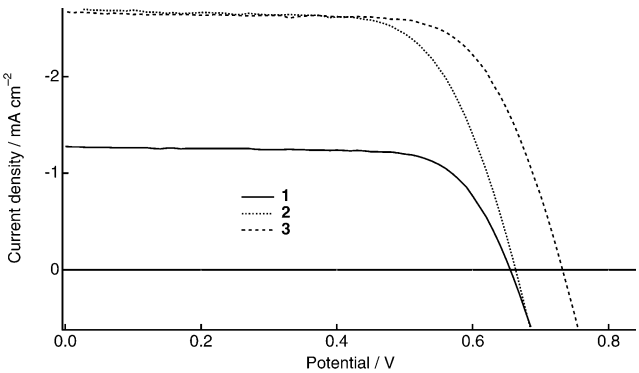

Figure 4. Photocurrent–voltage curves obtained with photovoltaic cells using different sensitizers: **1**, **2**, and **3**. Light source: solar simulator AM1.5 spectral distribution, intensity 300 $W\,m^{-2}$. Electrolyte consisted of $[Co^{II}$-$(dbbip)_2](ClO_4)_2$ (0.09 M) and the oxidized species (0.01 M) in acetonitrile/ethylene carbonate (40:60).

Figure 5 shows results from nanosecond time-resolved laser experiments. The transient absorbance signal measured at $\lambda = 630$ nm monitors the concentration of the oxidized sensitizer species produced on photoinduced electron injection into the

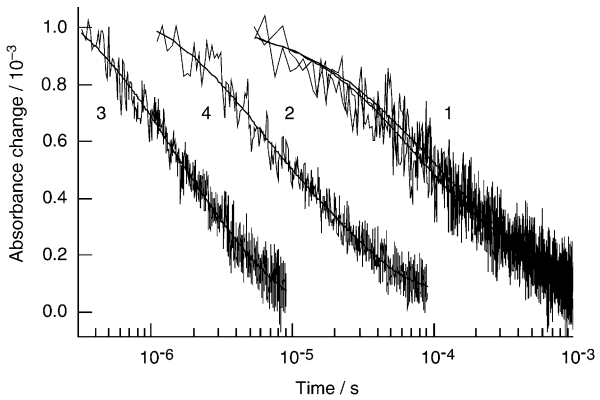

Figure 5. Time course of the transient absorbance changes obtained on nanosecond pulsed laser excitation ($\lambda = 510$ nm, 5 ns fwhm pulse duration, 30 mJ cm^{-2} pulse fluence) of dye sensitizers **1** (traces 1 and 3) and **3** (traces 2 and 4) adsorbed on mesoporous TiO_2 films. Transient absorbance signals were measured at $\lambda = 630$ nm in the presence of pure acetonitrile/ethylene carbonate (40:60; traces 1 and 2) and with addition of $[Co^{II}(dbbip)_2](ClO_4)_2$ (0.1M; traces 3 and 4).

TiO_2 conduction band. In the absence of the mediator, the decay of the signal recorded under open-circuit conditions was solely due to back electron transfer. The kinetics of this process were quite similar for dyes **1** and **3**, with half-reaction times on the order of $t_{1/2} = 100$ µs. As expected, the addition of the mediator $[Co^{II}(dbbip)_2](ClO_4)_2$ (0.1M) was observed to cause the efficient reduction of the sensitizer's oxidized species in kinetic competition with the above charge-recombination process. Surprisingly, the kinetics of dye regeneration were found to be clearly faster for sensitizer **1** ($t_{1/2} \approx 2$ µs) than for dye **3** ($t_{1/2} \approx 10$ µs). Although decay kinetics could not be described accurately by simple exponentials, the quantum yield Φ_r for dye cation interception by the mediator can be approximated by Equation (1), where k_r is the first-order rate constant for the reduction of the sensitizer's oxidized species by the mediator, and k_b the rate constant for back electron transfer from the conduction band to the same dye cations.

$$\Phi_r = \frac{k_r}{k_r + k_b} \quad (1)$$

Assuming in a crude approximation $k_b = 1/t_{1/2} \approx 10^4$ s^{-1}, $k_r(\mathbf{1}) = 1/t_{1/2}(\mathbf{1}) \approx 5 \times 10^5$ s^{-1}, and $k_r(\mathbf{3}) = 1/t_{1/2}(\mathbf{3}) \approx 10^5$ s^{-1}, interception quantum yields of $\Phi_r(\mathbf{1}) \approx 0.98$ and $\Phi_r(\mathbf{3}) \approx 0.91$ can be estimated for the two sensitizers. These results show that dye **1** suffers neither from faster back electron transfer nor from reduced interception efficiency. Kinetic parameters deduced from laser experiments therefore cannot be invoked to explain the lower photovoltaic performance of this sensitizer compared to the amphiphilic dye **3**.

The heteroleptic complex **3** carries two nonyl chains at the 4,4′-positions of the 2,2′-bipyiridine ligand. These groups may sterically hinder the approach of the cobalt complex, which has four butyl chains of its own. Complex **1** does not bear any alkyl chains, and its regeneration by Co^{2+} is indeed kinetically favored. The increase in photocurrent obtained on using dye **3** instead of **1** can be explained by other arguments: The TiO_2 surface covered by **1** carries more negative charges than in the case of **3**. Moreover, Co^{2+} can more closely approach the surface sensitized by **1** due to the weaker steric effect. Sensitizer **1** can therefore easily create an ion pair with the oxidized Co^{3+}, which can in turn intercept the electron from the excited dye or from the TiO_2 conduction band. This ion-pairing effect may also decrease Co^{3+} diffusion to the counterelectrode and therefore reduce the available photocurrent.[21] In the case of **3**, the ion-pairing effect is limited, and the current and voltage can be higher.

Photoanode optimization: Apart from the sensitizer, the photovoltaic performance of $[Co^{II/III}(dbbip)_2](ClO_4)_{2/3}$-based solar cells was found to be strongly influenced by the structure of the mesoporous TiO_2 films. The photoanode has a triple-layered structure, in which the first layer is a compact blocking TiO_2 film, the second a transparent TiO_2 layer with particles of about 20 nm, and the third a scattering film with large TiO_2 particles of 400 nm in diameter.

As shown in Table 2, the IPCE values and consequently the photocurrent decrease with increasing thickness of the nanocrystalline and scattering TiO_2 layers. Apparently, for thicker

Table 2. Photovoltaic data at 100 W m^{-2} for various thicknesses of TiO_2 layers.

Layer 1[a] [µm]	Layer 2[b] [µm]	V_{OC} [mV]	J_{SC} [mA cm^{-2}]	FF	η[c] [%]	IPCE[d] [%]
2	2	630	1.11	0.65	4.6	70
2	4	590	1.34	0.67	5.5	68
4	2	570	1.16	0.65	4.4	59
4	4	560	1.25	0.68	5.0	59
6	2	590	1.00	0.74	4.6	48
10	2.5	570	0.76	0.67	3.0	38

[a] Transparent mesoporous layer (particle ∅ 18 nm). [b] Scattering layer (particle ∅ 400 nm). [c] Efficiency. [d] IPCE at 540 nm.

films a significant fraction of the injected electrons recombine before reaching the collector electrode. Enhanced recombination is also responsible for the decreased open-circuit photovoltage V_{OC}. Surprisingly, the fill factor (FF) values appear to change only slightly for the different film thicknesses. However, interpretation should be made with caution, as the fill factor reflects relative losses due to internal cell resistance and hence is affected by both J_{SC} and V_{OC}.

Influence of underlayer and electrocatalysts: At the photoanode, the unwanted reduction of Co^{III} to Co^{II} at the transparent conductive glass (TCO, fluorine-doped SnO_2) may compete with the reduction of the complex by the oxidized dye. Evidence for Co^{III} reduction on the SnO_2 surface not covered by TiO_2 nanocrystals but exposed to the electrolyte is shown in Figure 6. Therefore, depositing a compact TiO_2 film on the conducting glass had a beneficial effect on the $I-V$ curves, and the absence of such a blocking layer induces a clear shunt. The presence of a compact underlayer is

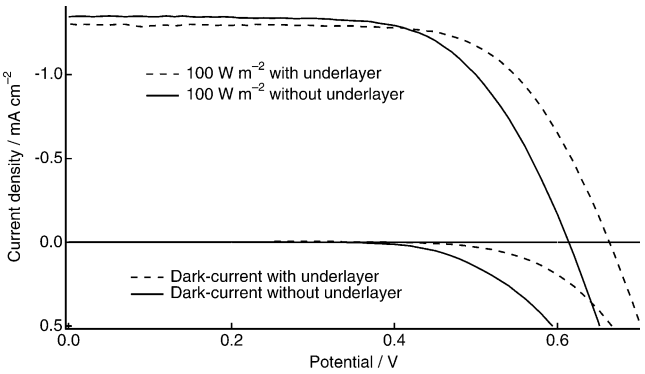

Figure 6. The influence of a compact TiO_2 underlayer on the dark current and the current at 100 W m^{-2}. Sensitizer **3** was used with the same electrolyte as in Figure 4.

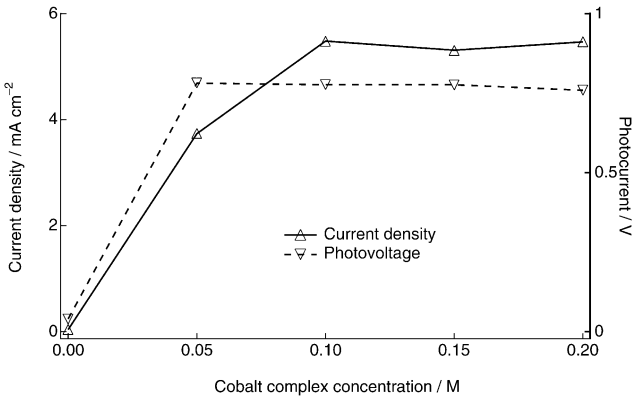

Figure 7. Influence of the redox mediator concentration on the current density and photovoltage measured under full AM1.5 sunlight. Efficiency and IPCE at 540 nm (not shown) exhibit the same behavior as current density and photovoltage, respectively. The Co^{III}/Co^{II} concentration ratio was maintained at 0.1.

therefore highly recommended when using cobalt complexes as redox mediators in liquid-electrolyte dye-sensitized solar cells.

If the $[Co^{III/II}(dbbip)_2]$ redox couple exhibits reversible electrochemical behavior on SnO_2, the reduction of Co^{III} to Co^{II} would be fast enough to render superfluous the use of additional electrocatalysts, such as platinum, on the counterelectrode. To test this hypothesis, TCO glass with and without catalytic coatings of platinum was examined as counterelectrode. The $I-V$ curves observed with untreated TCO glass showed a sigmoidal shape that indicated that the current is limited at low overvoltage by interfacial charge-transfer resistance. As a result, poor fill factors were obtained with the SnO_2 counterelectrode. Depositing electrocatalytic platinum on the SnO_2 film led to a marked improvement in the $I-V$ characteristics. In the absence of an appropriate electrocatalyst, fluorine-doped tin dioxide cannot function adequately as counterelectrode, despite the fact that the exchange current is higher for the $[Co^{III/II}(dbbip)_2]$ compared to the triiodide/iodide couple.

Optimization of redox mediator concentration and degree of oxidation: To test the effect of redox mediator concentration on the photovoltaic performance and on the dynamics of dye regeneration, four solutions with different concentrations of $[Co(dbbip)_2](ClO_4)_2$ (0.05, 0.10, 0.15 and 0.20 M) were prepared. They were all partially oxidized and contained 90% of $[Co(dbbip)_2]^{2+}$. As shown in Figure 7, the photovoltage is independent of the cobalt complex concentration above 0.05 M. In contrast, the efficiency increases from 3.7 to 5.5 mA cm^{-2} when the redox mediator concentration is increased from 0.05 to 0.10 M and then remains stable, the increase in conductivity being compensated by the increase in viscosity, which slows down the diffusion of the oxidized species.

The Co^{III}/Co^{II} concentration ratio is also expected to have an impact on photovoltaic performance. To quantify this effect and find the optimal degree of oxidation, four different electrolytes were prepared, each containing initially 0.1 M of $[Co(dbbip)_2](ClO_4)_2$, which was converted in varying proportions to Co^{III} by adding $NOBF_4$. A Co^{III}/Co^{II} ratio of 0.11 was found to be optimal. The current density is adversely affected by the presence of increasing Co^{III} concentrations, as shown in Figure 8, and this is attributed to the failure to intercept the back reaction. The regeneration of the dye by the Co^{II} complex may also be impaired by the association of Co^{III} with the sensitizer. The influence of Co^{III}/Co^{II} ratio on the kinetics of dye regeneration with $[Co(dmbip)_2](ClO_4)_2$ and **1** was monitored by laser flash photolysis experiments in a previous publication.[21]

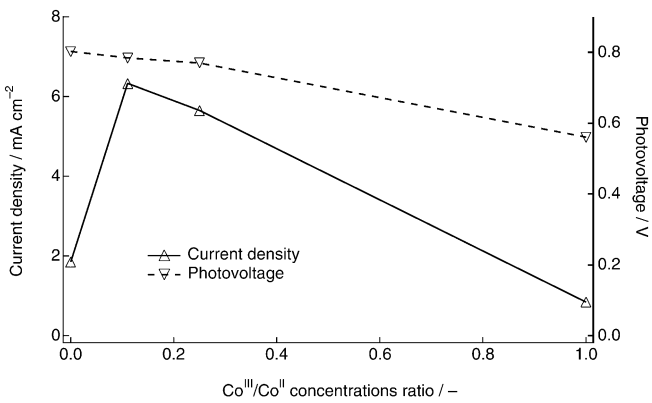

Figure 8. Influence of Co^{III}/Co^{II} concentration ratios on current density and photovoltage at 1000 W m^{-2} with **3** and the same electrolyte as in Figure 4. Efficiency and IPCE at 540 nm (not shown) exhibit the same behavior as current density and photovoltage, respectively.

Mass-transport effects: The variations of photocurrent as a function of irradiation intensity on illuminating a cell from the photoanode (PA) or counterelectrode (CE) side were studied. Mass-transport effects are clearly an issue for electrolytes based on cobalt complexes as redox mediators, in particular under full-sunlight illumination, for which the current densities exceed 5 mA cm^{-2}. In this case, both the oxidized and reduced complexes are subject to mass-transport limitation, while for triiodide/iodide-based electrolytes, diffusion restrictions on the current arise only for the triiodide ions.[35] As shown in Figure 9, in the low-current region PA illumination is superior. Due to the TiO_2 optical scattering layer deposited on the sensitized photoactive layer, CE-side light exposure

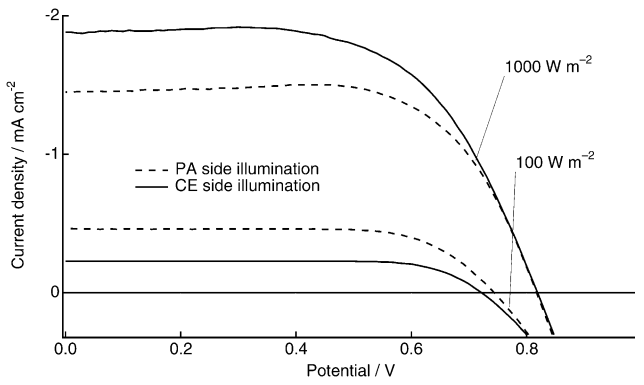

Figure 9. $I-V$ curves showing the differences between photoanode-side (PA) and counterelectrode-side (CE) illumination for irradiation at 1000 W m^{-2} and 100 W m^{-2}. Conditions are the same as in Figure 6.

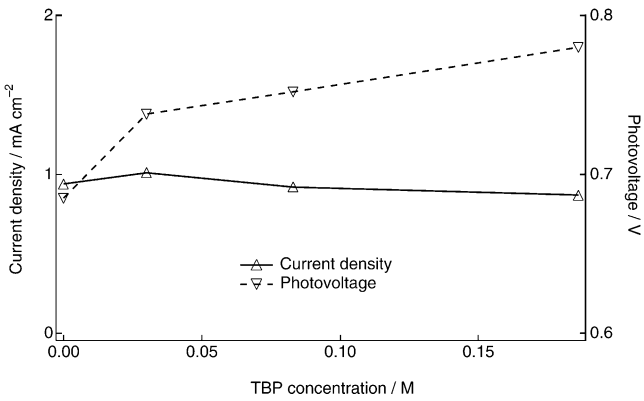

Figure 10. Effect of TBP concentration on current density and photovoltage at 100 W m^{-2}. Efficiency and IPCE at 540 nm (not shown) exhibit the same behavior as current density. Only the photovoltage continues to increases with increasing concentration of TBP. Conditions are the same as in Figure 6.

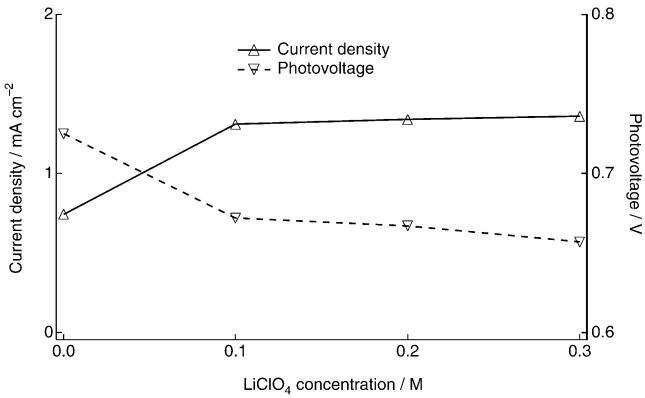

Figure 11. Effect of $LiClO_4$ concentration on current density and photovoltage at 100 W m^{-2}. Efficiency and IPCE at 540 nm (not shown) exhibit the same behavior as current density. Conditions are the same as in Figure 6.

results in reflection losses. This effect is overcompensated at high illumination intensity by the improvement in mass transport. Mass-transport limitation manifests itself as a deviation from a linear dependence of the current density on light intensity. The current density at which this takes place is much higher with CE irradiation than with PA irradiation. The implies that when the mass transport is limiting, it is preferable to provide irradiation from the CE side to improve the linearity of the performance with light intensity by alleviating the diffusion problems in the cell.

Additives: As was shown previously for the triiodide/iodide-based electrolytes,[36, 37] additives can be used to optimize the electrolyte composition and to improve the solar-cell performance. Our studies focused on 4-*tert*-butylpyridine (TBP) and lithium perchlorate. TBP is known to passivate recombination centers and therefore reduce back electron transfer in TiO_2, resulting in a higher open-circuit photovoltage. $LiClO_4$ in the electrolyte system increases the photocurrent, due to the adsorption of Li^+ on TiO_2 at high concentration,[37, 38] and shifts the flatband potential of TiO_2 to more positive values.[39] This effect enhances the charge-collection efficiency of the oxide film. Hence, it is important to use both TBP and $LiClO_4$ to increase the J_{SC} and V_{OC} values.

Measurements of $I-V$ and IPCE were carried out with electrolytes with varying concentrations of TBP or $LiClO_4$ (Figures 10 and 11). Addition of TBP increased the photovoltage by about 100 mV at 100 W m^{-2}. Addition of $LiClO_4$ nearly doubles the photocurrent at 100 W m^{-2}, while decreasing the photovoltage by less than 100 mV for any concentration. In general, this decrease in photovoltage by Li^+ addition is similar to that of classic triiodide/iodide-based liquid electrolytes, but less pronouced; a typical electrolyte based on triiodide/iodide in a nitrile solvent shows a decrease of at least 150 mV on addition of 0.1 M of Li^+. In contrast to our results, an increase in the photovoltage was observed by Sapp et al. on addition of Li^+ ions, which was attributed to an increase in the effective overpotential for reduction of the sensitizer at the photoelectrode on addition of Li^+ to the solution.[32] Typical results are presented in Table 3 for an optimized electrolyte containing 0.1 M of $[Co(dbbip)_2](ClO_4)_2$ and 0.01 M of $NOBF_4$ (10% oxidized species) in acetonitrile/ethylenecarbonate (40/60) with addition of 0.2 M $LiClO_4$ and 0.1 M TBP. The best result at full sun (1000 W m^{-2}) gave a J_{SC} of about 8–9 mA cm^{-2}, V_{OC} of 870 mV, FF of 0.55, and an efficiency greater than 4%. With the same electrolyte an IPCE of over 80% at 540 nm was obtained.

Table 3. Variations in photovoltaic performance parameters at three different illumination levels with an optimized electrolyte.

Power[a] [W m^{-2}]	V_{OC} [mV]	J_{SC} [mA cm^{-2}]	FF	η[b] [%]	IPCE[c] [%]
15	690	0.24	0.77	7.9	74
100	765	1.35	0.73	7.9	74
1000	840	8.40	0.56	3.9	74

[a] Incident illumination levels. [b] Efficiency. [c] IPCE at 540 nm with an illumination of 100 W m^{-2}.

Conclusion

Studies were performed on new redox mediator systems that could replace the triiodide/iodide couple in dye-sensitized nanocrystalline solar cells. The one-electron-transfer redox

mediator $[Co(dbbip)_2](ClO_4)_2$ performed best among the compounds investigated. The $E_{1/2}$ value of cobalt complexes influences V_{OC}, which increases with higher $E_{1/2}$ values. In spite of slow dye regeneration kinetics for **3**, the enhanced photovoltaic performance observed with this dye are due to steric and electrostatic effects. With the design of novel heteroleptic hydrophobic ruthenium dyes and optimized electrolyte solutions, we were able to reach incident photon-to-current conversion efficiencies of over 80% in the visible region. The overall AM1.5 solar-to-electric power conversion efficiency was 8% at 100 W m^{-2}. It decreases to about half of this value at full sunlight intensity, due to the diffusional limitation of the photocurrent at the counterelectrode.

Experimental Section

Materials: The solvents and salts used in this study (puriss. grade) were purchased from Fluka. The ruthenium sensitizers **1**–**3** were prepared as reported earlier.[3, 40] The ligands [2,6-bis(1′-methylbenzimidazol-2′-yl)pyridine] and 2,6-bis(1′-butylbenzimidazol-2′-yl)pyridine were synthesized according to reported procedures.[41, 42] The cobalt complexes $[Co(terpy)_2](ClO_4)_2$, $[Co(bipy)_3](ClO_4)_2$, $[Co(phen)_3](OTf)_2$, $[Co(dbbip)_2](ClO_4)_2$, $[Co(dmbip)_2](ClO_4)_2$, $[Co(dmbip)_2](DDS)_2$ and $[Co(dmbip)_2](PF_6)_2$ (bipy = 2,2′-bipyridine, phen = 1,10-phenanthroline, dbbip = 2,6-bis(1′-butylbenzimidazol-2′-yl)pyridine, dmbip = [2,6-bis(1′-methylbenzimidazol-2′-yl)pyridine], OTf^- = trifluoromethanesulfonate ($CF_3SO_3^-$), DDS^- = dodecylsulfate) were synthesized according to reported procedures.[43–45]

In a typical synthesis, a solution of $CoCl_2$ (0.25 g, 1.05 mmol) in water was added dropwise to an ethanolic solution of ligand (2.11 mmol of terpy, dbbip or dmbip; 3.15 mmol of bipy or phen) to give a yellow solution. Then the CoL_2^{2+} or CoL_3^{2+} complex was precipitated by addition of an aqueous saturated solution of the required anion. The compound was collected by filtration, washed thoroughly with water and diethyl ether and dried under vacuum.

Analytical measurements: UV/Vis spectra were recorded in a quartz cell with 1 cm path length on a HP 8453 spectrophotometer. Electrochemical redox potentials were obtained by stationary amperometry using a single-compartment three-electrode cell and a standard potentiostat. The working electrode was a nominal 10 μm diameter Pt ultramicroelectrode (UME), the auxiliary electrode was a platinum wire, the reference electrode was a silver wire, and the electrolyte was a solution of tetrabutylammonium hexafluorophosphate ($TBAPF_6$) in acetonitrile (0.01M).

The diffusion coefficient of $[Co(dbbip)_2](ClO_4)_2$ was measured using a two-electrode cell with an Autolab potentiostat. The working electrode was a Pt UME with a measured diameter of 10.9 μm, and the counterelectrode a platinum wire. The electrolyte was the same as for the redox potential measurements.

Proton and ^{13}C NMR spectra were measured on a Bruker 200 MHz spectrometer. The reported chemical shifts are relative to TMS.

Elemental analysis (C, H, N) was performed by Ilse Beetz Mikroanalytisches Laboratorium, Germany.

X-ray single-crystal diffraction studies were performed by Y. L. Slovokhotov and I. S. Neretin on a 110 K Bruker SMART diffractometer with a sealed X-ray tube. These measurements were carried out in the Laboratory of Polymer Structural Studies, Institute of Organoelement Compounds, Russian Academy of Sciences, Moscow.

Electrolyte preparation: Electrolyte solutions were prepared by dissolving a certain amount of cobalt complex redox mediator in anhydrous acetonitrile/ethylene carbonate (40:60). This solvent mixture was used for all the experiments described hereafter. Partial oxidation of Co^{II} complex to Co^{III} was achieved by adding stoichiometric amounts of solid $NOBF_4$, a one-electron acceptor, to the mediator solution. The influence of Co^{II} and Co^{III} concentrations, as well as that of other additives on the photovoltaic performance is discussed in the corresponding sections. If not otherwise specified the concentrations of Co^{II} and Co^{III} complexes used were 9×10^{-2} and 1×10^{-2} M, respectively.

Photoelectrode preparation: Photoelectrodes consisted of a TiO_2 film with a triple-layer structure. A compact blocking underlayer of spray-pyrolyzed titanium dioxide (ca. 150 nm thick) was deposited onto a cleaned conducting glass substrate (NSG, F-doped SnO_2, resistance 10 Ω sq^{-1}). A solution of titanium diisopropoxide bis(acetylacetonate) in ethanol (0.2 M) was sprayed 15 times over the conducting glass surface, which was maintained at 400 °C. Treated glass plates were fired at 500 °C for 30 min to remove remaining organic traces. Successive depositions of a 2 μm thick transparent layer and a 4 μm thick light-scattering layer of nanocrystalline TiO_2, prepared as reported earlier,[46] and final post-treatment with an aqueous solution of $TiCl_4$ were then carried out according to a previously published procedure.[21] Dye derivatization of nanocrystalline oxide films was obtained by immersion of electrodes, heated beforehand under oxygen at 500 °C for 15 min, in acetonitrile/*tert*-butanol (1:1) sensitizer solutions (5×10^{-4} M). Sensitized semiconductor films were finally pressed against a reflective platinum counterelectrode on which a drop of the electrolyte was deposited. A mask was applied on the photoactive surface to define a well known area of 0.44 cm^2 for each cell. The method used to collect photoelectrochemical data was discussed in a previous publication.[47] At least three cells were measured for each experiment, and the average values are reported. Experimental errors on the photovoltaic measurements are in the range of ±5%.

Laser flash photolysis: Transparent mesoporous TiO_2 layers (thickness 5 μm) were prepared on a glass substrate. Dry nanocrystalline TiO_2 films were dyed by adsorption of the sensitizers. A drop of pure solvent mixture (acetonitrile/ethylene carbonate 40:60) or of electrolyte containing $[Co^{II}(dbbip)_2](ClO_4)_2$ (0.1 M) was then sandwiched between the sample and a thin microscope cover glass. Samples were subjected to low-intensity flash photolysis immediately after preparation. Pulsed laser excitation was applied using a broadband optical parametric oscillator pumped by a frequency-tripled Q-switched Nd:YAG laser (30 Hz repetition rate, pulse width at half-height 5 ns) The output of the OPO was tuned to $\lambda = 510$ nm and attenuated by filters. The beam was expanded by a planoconcave lens to irradiate a large cross section (ca. 1 cm^2) of the sample, whose surface was kept at a 30° angle to the excitation beam. The analyzer light, produced by a cw Xe arc lamp, was passed through a first monochromator, various optical elements, the sample, and a second monochromator prior to being detected by a fast photomultiplier tube. Signals were measured at $\lambda =$ 630 nm in order to monitor the oxidized-dye concentration. Satisfactory signal-to-noise ratios were typically obtained by averaging more than one thousand laser shots.

Acknowledgements

Financial support of this work by the Swiss National Science Foundation (FNRS), Aisin Seiko Co. Ltd, Japan, and its European subsidiary IMRA Europe SA, France, is gratefully acknowledged, as well as P. Comte for the preparation of TiO_2 films, N. Eugster, D. Fermín, P. Wang for their help in electrochemistry (ICMB, Swiss Federal Institute of Technology, Lausanne), and Y. L. Slovokhotov and I. S. Neretin for crystal structure determination (Russian Academy of Sciences, Moscow).

[1] M. K. Nazeeruddin, A. Kay, I. Rodicio, R. Humphry-Baker, E. Müller, P. Liska, N. Vlachopoulos, M. Grätzel, *J. Am. Chem. Soc.* **1993**, *115*, 6382–6390.

[2] M. K. Nazeeruddin, P. Péchy, M. Grätzel, *Chem. Commun.* **1997**, 1705–1706.

[3] M. K. Nazeeruddin, S. M. Zakeeruddin, R. Humphry-Baker, M. Jirousek, P. Liska, N. Vlachopoulos, V. Shklover, C.-H. Fischer, M. Grätzel, *Inorg. Chem.* **1999**, *38*, 6298–6305.

[4] S. M. Zakeeruddin, M. K. Nazeeruddin, P. Péchy, F. P. Rotzinger, R. Humphry-Baker, K. Kalyanasundaram, M. Grätzel, V. Shklover, T. Haibach, *Inorg. Chem.* **1997**, *36*, 5937–5946.

[5] K. Tennakone, G. R. R. A. Kumara, P. M. Sirimanne, K. G. U. Wijayantha, *Photochem. Photobiol. A* **1996**, *94*, 217–220.

[6] M. Yanagida, L. P. Singh, K. Sayama, K. Hara, R. Katoh, A. Islam, H. Sugihara, H. Arakawa, M. K. Nazeeruddin, M. Grätzel, *J. Chem. Soc. Dalton Trans.* **2000**, 2817 – 2822.
[7] K. Hara, T. Horiguchi, T. Kinoshita, K. Sayama, H. Sugihara, H. Arakawa, *Sol. Energy Mater.* **2000**, *64*, 115 – 134.
[8] A. Ehret, L.Stuhl, M. T. Spitler, *J. Phys. Chem. B* **2001**, *105*, 9960 – 9965.
[9] G. Sauve, M. E. Cass, S. J. Doig, I. Lauermann, K. Pomykal, N. S. Lewis, *J. Phys. Chem. B* **2000**, *104*, 3488 – 3491.
[10] C. J. Barbé, F. Arendse, P. Comte, M. Jirousek, F. Lenzmann, V. Shklover, M. Grätzel, *J. Am. Ceram. Soc* **1997**, *80*, 3157 – 3171.
[11] S. D. Burnside, V. Shklover, C. Barbé, P. Comte, F. Arendse, K. Brooks, M. Grätzel, *Chem. Mater.* **1998**, *10*, 2419 – 2425.
[12] N.-G. Park, J. v. d. Lagemaat, A. J. Franck, *J. Phys. Chem. B* **2000**, *104*, 8989 – 8994.
[13] F. Lenzmann, J. Krueger, S. Burnside, K. Brooks, M. Grätzel, D. Gal, S. Rühle, D. Cahen, *J. Phys. Chem. B* **2001**, *105*, 6347 – 6352.
[14] K. Srikanth, M. M. Rahman, H. Tanaka, K. M. Krishna, T. Soga, M. K. Mishra, T. Jimbo, M. Umeno, *Sol. Energy Mater.* **2001**, *65*, 171 – 177.
[15] P. Bonhôte, A.-P. Dias, N. Papageorgiou, K. Kalyanasundaram, M. Grätzel, *Inog. Chem.* **1996**, *35*, 1168 – 1178.
[16] N. Papageorgiou, Y. Athanassov, M. Armand, P. Bonhôte, H. Pettersson, A. Azam, M. Grätzel, *J. Electrochem. Soc.* **1996**, *143*, 3099 – 3108.
[17] E. Stathatos, P. Lianos, C. Krontiras, *J. Phys. Chem. B* **2001**, *105*, 3486 – 3492.
[18] S. Mikoshiba, H. Sumino, M. Yonetsu, S. Hayase, "Highly Efficient Photoelectrochemical Cell with Novel Polymer Gel Electrolytes", *16th European Photovoltaic Solar Energy Conference and Exhibition*, Glasgow, **2000**.
[19] A. F. Nogueira, M.-A. D. Paoli, *Sol. Energy Mater.* **2000**, *61*, 135 – 141.
[20] G. Oskam, B. V. Bergeron, G. J. Meyer, P. C. Searson, *J. Phys. Chem. B* **2001**, *105*, 6867 – 6873.
[21] H. Nusbaumer, J. E. Moser, S. M. Zakeeruddin, M. K. Nazeeruddin, M. Grätzel, *J. Phys. Chem. B* **2001**, *105*, 10461 – 10464.
[22] P. Wang, S. M. Zakeeruddin, I. Exnar, M. Grätzel, *Chem. Commun.* **2002**, 2972 – 2973.
[23] P. Wang, S. M. Zakeeruddin, P. Comte, I. Exnar, M. Grätzel, *J. Am. Chem. Soc.* **2003**, *125*, 1166 – 1167.
[24] F. Cao, G. Oskam, G. J. Meyer, P. C. Searson, *J. Phys. Chem. B* **1996**, *100*, 17021 – 17027.
[25] H. Wang, J. He, G. Boschloo, H. Lindström, A. Hagfeldt, S.-E. Lindquist, *J. Phys. Chem. B* **2001**, *105*, 2529 – 2533.
[26] N. W. Duffy, L. M. Peter, K. G. U. Wijayantha, *Electrochem. Commun.* **2000**, *2*, 262 – 266.
[27] O. Kohle, M. Grätzel, A. F. Meyer, T. B. Meyer, *Adv. Mater.* **1997**, *9*, 904 – 906.
[28] H. Greijer, J. Lindgren, A. Hagfeldt, *J. Phys. Chem. B* **2001**, *105*, 6314 – 6320.
[29] M. Amirnasr, M. K. Nazeeruddin, M. Grätzel, *Thermochim. Acta* **2000**, *348*, 105 – 114.
[30] M. Grätzel, *Pure Appl. Chem.* **2001**, *73*, 459 – 467.
[31] C. Nasr, S. Hotchandani, P. V. Kamat, *J. Phys. Chem. B* **1998**, *102*, 4944 – 4951.
[32] S. A. Sapp, C. M. Elliott, C. Contado, S. Caramori, C. A. Bignozzi, *J. Am. Chem. Soc.* **2002**, *124*, 11215 – 11222.
[33] Y. L. Slovokhotov, H. Nusbaumer, S. M. Zakeeruddin, I. S. Neretin, V. Shklover, M. Grätzel, unpublished results.
[34] S. Pelet, J. E. Moser, M. Grätzel, *J. Phys. Chem. B* **2000**, *104*, 1791 – 1795.
[35] N. Papageorgiou, M. Grätzel, P. Infelta, *Sol. Energy Mater.* **1996**, *44*, 405 – 438.
[36] S. Y. Huang, G. Schlichthörl, A. J. Nozik, M. Grätzel, A. J. Franck, *J. Phys. Chem. B* **1997**, *101*, 2576 – 2582.
[37] S. Nakade, S. Kambe, T. Kitamura, Y. Wada, S. Yanagida, *J. Phys. Chem. B* **2001**, *105*, 9150 – 9152.
[38] S. Kambe, S. Nakade, T. Kitamura, Y. Wada, S. Yanagida, *J. Phys. Chem. B* **2002**, *106*, 2967 – 2972.
[39] B. Enright, G. Redmond, D. Fitzmaurice, *J. Phys. Chem.* **1994**, *98*, 6195 – 6200.
[40] S. M. Zakeeruddin, M. K. Nazeeruddin, R. Humphry-Baker, P. Péchy, P. Quagliotto, C. Barolo, G. Viscardi, M. Grätzel, *Langmuir* **2002**, *18*, 952 – 954.
[41] C. Piguet, B. Bocquet, E. Müller, A. F. Williams, *Helv. Chim. Acta* **1989**, *72*, 323.
[42] W. Addison, P. J. Burke, *J. Heterocycl. Chem.* **1981**, *18*, 803.
[43] V. Shklover, I. L. Eremenko, H. Berke, R. Nesper, S. M. Zakeeruddin, M. K. Nazeeruddin, M. Grätzel, *Inorg. Chim. Acta* **1994**, *219*, 11 – 21.
[44] J. M. Dekorte, G. D. Owens, D. W. Margerum, *Inog. Chem.* **1979**, *18*, 15381.
[45] D. J. Szalda, C. Creutz, D. Mahajan, N. Sutin, *Inog. Chem.* **1983**, *22*, 2372.
[46] M. Grätzel, *J. Sol-Gel Sci. Technol.* **2001**, *22*, 7 – 13.
[47] M. K. Nazeeruddin, P. Péchy, T. Renouard, S. M. Zakeeruddin, R. Humphry-Baker, P. Comte, P. Liska, L. Cevey, E. Costa, V. Shklover, L. Spiccia, G. B. Deacon, C. A. Bignozzi, M. Grätzel, *J. Am. Chem. Soc.* **2001**, *123*, 1613 – 1624.

Received: November 14, 2002
Revised: May 5, 2003 [F4577]

